

Percolation on a multifractal

G. Corso, J. E. Freitas, L. S. Lucena, and R. F. Soares

*International Center for Complex Systems and Departamento de Física Teórica e Experimental,
Universidade Federal do Rio Grande do Norte, Campus Universitário 59078 970, Natal, RN, Brazil*

(Received 19 December 2002; revised manuscript received 9 April 2003; published 23 June 2004)

We investigate percolation phenomena in multifractal objects that are built in a simple way. In these objects the multifractality comes directly from the geometric tiling. We identify some differences between percolation in the proposed multifractals and in a regular lattice. There are basically two sources of these differences. The first is related to the coordination number, which changes along the multifractal. The second comes from the way the weight of each cell in the multifractal affects the percolation cluster. We use many samples of finite size lattices and draw the histogram of percolating lattices against site occupation probability. Depending on a parameter characterizing the multifractal and the lattice size, the histogram can have two peaks. We observe that the percolation threshold for the multifractal is lower than that for the square lattice. We compute the fractal dimension of the percolating cluster and the critical exponent β . Despite the topological differences, we find that the percolation in a multifractal support is in the same universality class as standard percolation.

DOI: 10.1103/PhysRevE.69.066135

PACS number(s): 64.60.Ak, 61.43.Hv, 05.40.-a, 91.60.-x

I. INTRODUCTION

Percolation theory has been used in several fields such as chemistry, epidemics, science of materials, transport of fluids in porous media, branched polymers, and econo-physics [1–8]. The original percolation model based on a square lattice has been extended to several kinds of regular and random lattice, to continuous media where the objects overlap in space, and to other complex systems [9–12]. In this work we generalize percolation theory to cover an even broader range of complex systems. We devise an approach to investigate how percolation occurs in a support that is itself a multifractal. For this purpose we have constructed an easily assembled multifractal immersed in a two-dimensional (2D) space.

Our work is inspired by the modeling of geophysical natural objects that show multifractal properties [13–16]. The model can be applied to transport of fluid in multifractal porous media such as sedimentary strata. Oil reservoirs are possible candidates to be modeled in such a way since the measurement of some physical quantities in well logs shows multifractal behavior [17,18]. Despite the potential applications, this problem is important by itself in the scientific context. The study of percolation phenomena in multifractal lattices is relevant in statistical physics, especially when the size of the blocks and their number of neighbors can vary.

In order to make this analysis we create a multifractal object that can be used as a toy model and a laboratory for percolation theory. An important characteristic of this object is that its topological properties (e.g., number of neighbors of each block) change over the object. In Ref. [19] an algorithm that has some resemblance to ours is used. That multifractal is built from the partition of a square, but the object has a trivial topology. In addition, the object used in [19] is stochastic and ours is deterministic. Although both models present multifractality, our model has the following differences: it shows a nontrivial topology, we can determine its spectrum of fractal dimensions analytically, it generalizes the square lattice, and it shows simplicity in construction.

The multifractal object we have developed is a natural generalization of the regular square lattice once we consider the algorithmic point of view. The algorithm that generates a square lattice with $2^n \times 2^n$ cells starting with a square of fixed size is the following. We begin with an $L \times L$ square and cut it into four identical pieces (cells). At each step all the cells are equally divided into four parts using vertical and horizontal segments. This process produces a lattice as a partition of the square. The multifractal we create is also a partition of the square, but the ratio in which we divide the cells is different from $1/2$. The parameter characterizing the multifractal, ρ , is related to the ratio of this division.

What makes this problem appealing to physics is the following. The support of the percolation clusters is composed of subsets of different fractal dimensions. It is important to know how these different subsets are connected and how they participate in the conducting process. There are intriguing features in the network due to the fact that all the cells have rectangular shape but the area and the number of neighbors can vary, forming an exotic tiling.

In Sec. II we present the multifractal object that we construct to study percolation, and we analyze how its multifractal partition maps into the square lattice. In Sec. III we expose the algorithm we use to estimate the percolation threshold and derive the multifractal spectrum of the multifractal object. In Sec. IV we show the numerical results and discuss the histograms of percolating lattices versus occupation probability. Finally, in Sec. V we summarize the main differences between percolation in a regular lattice and in a multifractal support.

II. THE MULTIFRACTAL OBJECT Q_{mf}

The central object of our analysis is a multifractal object that we call Q_{mf} . Before defining it we enumerate some of its properties.

(1) Q_{mf} is a multifractal, which means that Q_{mf} has an infinite number of k subsets each one with a distinct fractal dimension D_k .

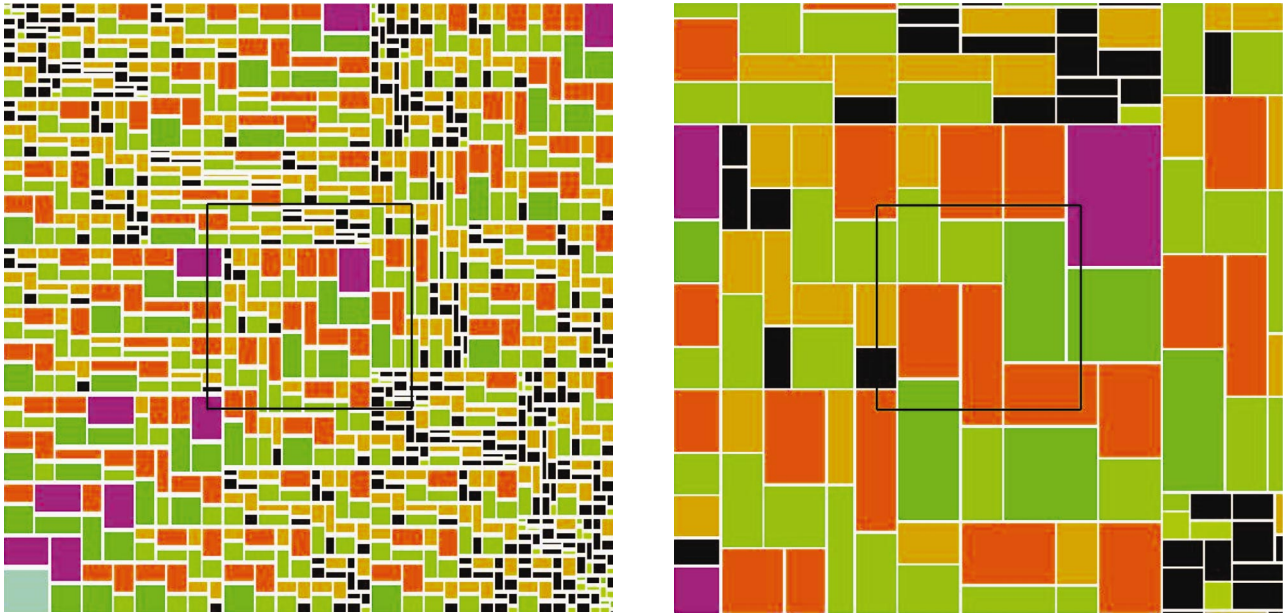


FIG. 2. (Color) The figure shows two views of the multifractal Q_{mf} for $n = 12$, $(s, r) = (3, 2)$. On the left we have the original picture. The right-hand panel is an enlargement of the square indicated at left.

$$D_X = \lim_{\epsilon \rightarrow 0} \frac{\log N(X)}{\log(1/\epsilon)} = \lim_{L \rightarrow \infty} \frac{\log N(X)}{\log L} \quad (3)$$

is finite, then D_X is the dimension of X .

In our case the object X is a k set. Remember that the k set corresponds to a set of rectangles of the same area. For a k set we have that N_k is given by

$$N_k = C_n^k s^k r^{(n-k)}, \quad (4)$$

where C_n^k is the binomial coefficient that express the number of elements of k type, and $s^k r^{(n-k)}$ is the area of each element of this set. If the square is partitioned n times ($n/2$ horizontal cuts and $n/2$ vertical cuts) its size is $L = (s+r)^{n/2}$. Combining all this information we have for the fractal dimension of each k set

$$D_k = \lim_{n \rightarrow \infty} \frac{\log C_n^k s^k r^{(n-k)}}{\log (s+r)^{n/2}}. \quad (5)$$

In the $r=s=1$ case all subsets of Q_{mf} are composed of elements of the same area, square cells. In this way the object is formed by a single subset with dimension

$$D = \lim_{n \rightarrow \infty} \frac{\log(1+1)^n}{\log(1+1)^{n/2}} = 2. \quad (6)$$

This result is expected since in this particular case Q_{mf} degenerates into a square lattice that has dimension 2.

In Fig. 2 we show the picture of Q_{mf} for $\rho = 2/3$. We have used $n = 12$. On the left, the full object is shown; on the right, an enlargement of an internal square of the object is illustrated. We have used the same color to indicate the elements of the same k set. The unusual tiling depicted in the figure is common for Q_{mf} 's with different values of ρ .

Figure 3 shows the spectrum of D_k for $n = 400$ calculated from Eq. (5). The use of increasing n does not change the shape of the curve, it only increases the number of k and makes the curve appear more dense. We use $(s, r) = (2, 3)$ to illustrate the asymmetry of the distribution. The spectrum has a maximum close to ρn . In this case $(2/3)400 \approx 270$. This means that the majority of the mass of the multifractal is concentrated in the k sets around this value. The spectrum D_k is typically asymmetric around its maximum. Only the case $(s, r) = (1, 1)$ is symmetric and the asymmetry of D_k increases as $s/(s+r) \rightarrow 1$, which is related to the area distribution among the blocks, as we shall see in the next section.

IV. NUMERICAL SIMULATIONS

In this section we focus our attention on the numerical results obtained from the algorithm exposed above. We are

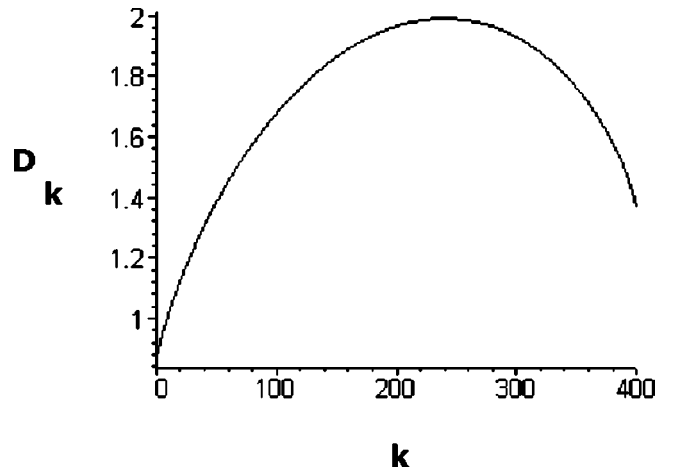


FIG. 3. The spectrum of fractal dimensions D_k of Q_{mf} for $n = 400$ and $(p, q) = (3, 2)$.

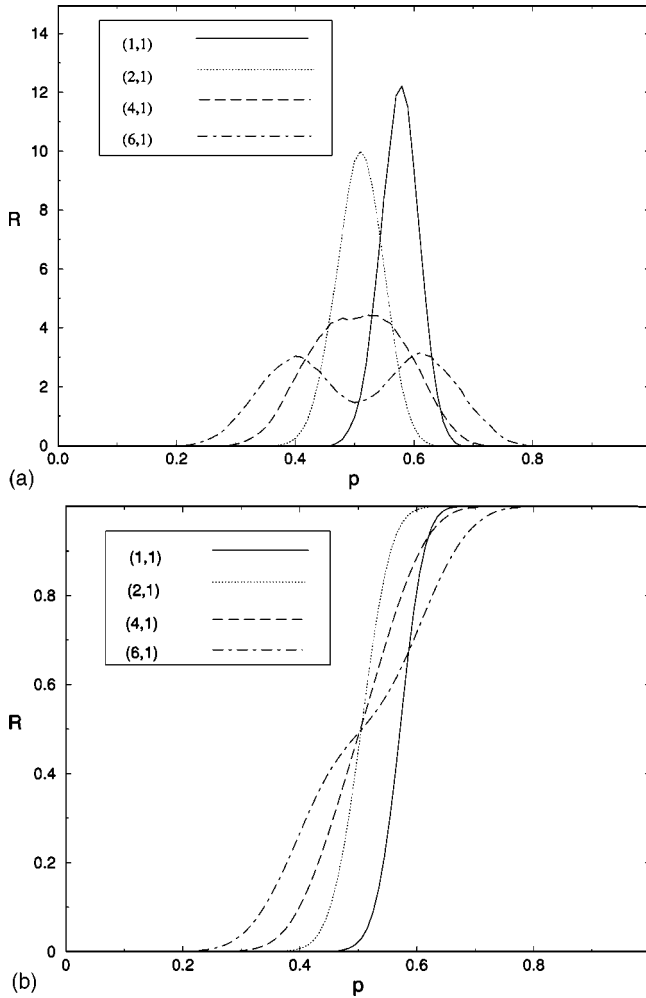


FIG. 4. In (a) is depicted the histogram of percolation lattices versus the occupation probability p for the cases $(s,r)=(1,1)$, $(2,1)$, $(4,1)$, and $(6,1)$. The areas under the curve are normalized to unity. For the same (s,r) a graphic of the fraction of percolation lattices R_L versus p is shown in (b). 40 000 lattices were used to make the average.

interested mainly in analyzing the percolating properties of Q_{mf} . Figure 4(a) shows the histogram of percolating lattices versus the occupation probability p . The area under the histogram is normalized to unity. We use $n = 10$ and average the results over 40 000 samples. We consider that a lattice percolates when it percolates from top to bottom or from left to right. The histogram of percolating lattices in both directions is similar but slightly shifted to the right. This shift is common in percolation (see Ref. [21] for percolation in a square lattice).

We show in Fig. 4(a) the results of simulations for the following values of (s,r) : $(1,1)$, which degenerates into the square lattice; and $(2,1)$, $(4,1)$, and $(6,1)$ which correspond to true multifractals. In this figure the histograms corresponding to $(2,1)$, $(4,1)$, and $(6,1)$ are shifted to the left compared to the histogram of $(1,1)$. The peak of the histogram for $(1,1)$ corresponds, as expected, to the square lattice size percolation threshold $p_c = 0.597$ [2], since this case matches the

TABLE I. The values of p_c , d_f , and β for several multifractals characterized by different pairs (s, r) .

(s,r)	(1,1)	(2,1)	(3,1)	(3,2)	(4,1)	(5,1)	(6,1)
p_c	0.593	0.527	0.526	0.526	0.525	0.525	0.530
d_f	1.895	1.900	1.911	1.890	1.902	1.929	1.842
β	0.127	0.128	0.140	0.141	0.141	0.118	0.109

square lattice exactly. The other values of p_c are shown in Table I.

The reason why Q_{mf} , for diverse ρ , shows roughly the same p_c comes from the topology of the multifractal. The topology of a set of blocks is related to the coordination number c , which is defined as the number of neighbors of each block [2]. Q_{mf} has the property that c changes along the object and with ρ . However, we compute the average coordination number c_{av} . These results do not depend significantly on ρ , or on n , the number of steps used to build Q_{mf} , which determines the number of blocks. The value found, $c_{av} = 5.436$, for the multifractal is close to the value of c for the triangular percolation problem, which has $c = 6$ and whose analytic percolation threshold is $p_c = 0.5$. The situation $(s,r) = (1,1)$, the square lattice, trivially shows $c = 4$. Because the square lattice has a different c it configures a particular situation compared to other Q_{mf} 's and it shows a different p_c as depicted in Fig. 4(a).

In Table I we show p_c and the fractal dimension of the percolating cluster, d_f , for diverse ρ . We have done an average over 100 000 samples and $n = 16$. The estimation of d_f is done by the relation $M \sim L^{d_f}$ for the “mass” M of the percolation cluster, which means the area of the cluster measured in units of the underlying square lattice, and L , the size of the underlying lattice. Based on the values of d_f of Table I we conclude that percolation on a multifractal support (embedded in two dimensions) belongs to the same class of universality as the usual percolation in two dimensions. The calculated value of d_f for the $(6,1)$ case is smaller compared to the others because of finite size effects. We discuss this effect in detail in the following paragraphs.

Percolation shows critical phenomena and several scaling relations are observed. The critical exponent β is defined from the equation

$$R_L \sim [p_c(L) - p_c]^\beta, \quad (7)$$

where p_c is the exact occupation probability value, in contrast to $p_c(L)$, which is the finite size value. The power law (7) is satisfied for $p_c(L)$ obtained from R_L . The numerical estimation of β is based on Eq. (7), where R_L is a key element of the analysis. For Q_{mf} the probability R_L is not a well behaved function of p for low L as we shall see in the next paragraphs. Actually, R_L can show, depending on ρ , an inflection point at p_c in this regime. However, in the case where $L \rightarrow \infty$ the scaling of $[p_c(L) - p_c]$ recovers the usual behavior. In this regime we find the same β characteristic of the two-dimensional case, $\beta = 5/36 = 0.13888$. We checked in our simulations that, for $n = 18$, β is around 5% of the exact value. The full set of values of β is in Table I.

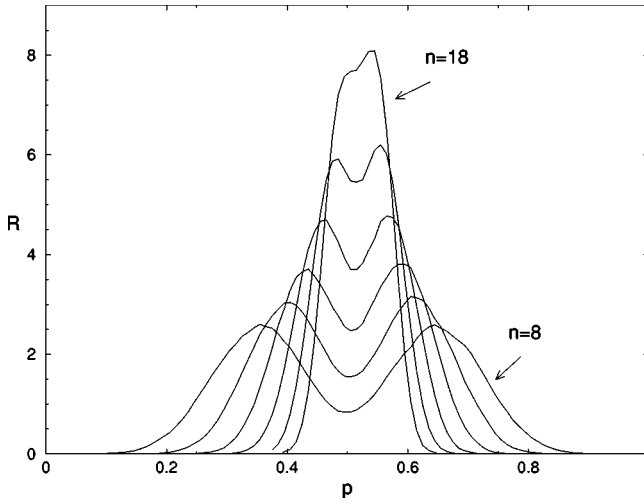


FIG. 5. The histogram of percolating lattices versus the occupation probability p for several values of the lattice size. The graphic shows the double peaks approaching each other as n increases. In the figure $(s,r)=(1,6)$ and $8 < n < 18$. 40 000 lattices were used to make the average.

It is worth saying that, despite small fluctuations in the values shown in the table, there is no trend in the numbers. The conclusion we take from these data is that the errors are caused by finite size effects and low-number statistics.

The dispersion of the histogram changes significantly with (s,r) as intuitively expected. To illustrate the change in the width of the histogram of a generic (s,r) multifractal we analyze the area of its blocks. At step n of the construction of Q_{mf} the largest element has the area $s^n/(s+r)^n$ and the smallest $r^n/(s+r)^n$ (using L^2 units). In this way the largest area ratio among blocks increases with $(s/r)^n$. As the occupation probability, entering in the percolation algorithm, is in general proportional to the area of the blocks, we expect that the width of the histograms in Fig. 4(a) increases with $(s/r)^n$. This increase in the dispersion is visualized clearly in the curves (2,1) and (4,1) of the figure.

The most singular curve in Fig. 4(a) is (6,1), which clearly shows two peaks. We stress this point when we comment on Fig. 5. Figure 4(b) uses the same data of as Fig. 4(a), but instead of the histogram of percolating lattices we show the cumulative sum R_L . As R_L is normalized, this parameter is also called the fraction of percolating lattices. As in Fig. 4(a) the case $(s,r)=(1,1)$, the square lattice, reproduces the results in the literature [21]. In this situation the lattice size L is $L=(s+r)^{10}=1024$. For this special case the number of blocks is equal to the number of unit boxes covering the surface. The double peak case $(s,r)=(6,1)$ shows an inflection point in the graphic of R_L versus p . In the following figure we explore this point in detail.

The most noticeable signature of percolation in the multifractal Q_{mf} is the double peak observed for $(s,r)=(6,1)$ in Fig. 5. In this figure the histogram of the percolating lattice versus p is plotted for diverse n as indicated in the figure. The distance between the peaks decreases as n increases. This picture indicates that the double peak is a phenomenon that is relevant for percolation in the multifractal, when ρ is

TABLE II. Estimation of Δp_{max} and $[s/(s+r)]^n$ for several steps n .

n	8	10	12	14	16	18
Δp_{max}	0.29	0.22	0.15	0.11	0.070	0.040
$\left(\frac{s}{s+r}\right)^n$	0.291	0.211	0.157	0.115	0.084	0.062

low, in the finite lattice size condition used in the simulation. From an analytic point of view the curve (6,1) in Fig. 5 is different from curve (1,1). In curve (6,1) there are three extremal points while in the (1,1) case the curve shows a single maximum point. We conjecture that in the limit of $n \rightarrow \infty$ these three points coalesce into a single one and all the curves show a similar behavior.

The two peaks in the histogram come from the huge difference among the area of the blocks of Q_{mf} . For large $(s/r)^n$ the area difference is so accentuated that we model the histogram of percolating lattices with bimodal statistics. In the case of the largest block chosen the multifractal easily percolates compared with the opposite possibility. To estimate the effect of the largest area block on the statistics we use Table II. The difference between the first peak at p_1 and the second one at p_2 is Δp_{max} . In Table II we compare Δp_{max} with the fraction of the largest block over the total square area $[s/(s+r)]^n$. This comparison is made for different steps in the construction of the multifractal n ; as n increases the area difference decreases as does the distance between peaks. Table II shows good agreement between the two values; we conclude that the bimodal statistic is caused by the huge mass of the largest block.

We notice, however, that the agreement between Δp_{max} and $[s/(s+r)]^n$ decreases as n increases. We interpret the disagreement between the bimodal statistics hypothesis and the numerics for high n as the limit of the hypothesis. Actually, the largest block is not the only one that produces anisotropy in the multifractal, and as n increases this fact becomes more accentuated. For small n the large block can be taken as the main factor in the anisotropy, and the bimodal statistics apply. Large n implies, however, true multifractals and a more complex statistics should be used to treat the problem.

V. CONCLUSION

In this work we develop a multifractal object Q_{mf} to study percolation in a multifractal support. In addition to being a multifractal, Q_{mf} shows several interesting properties. The sum of all its fractal subsets fills a square, and it is possible to determine the spectrum of its fractal dimensions. In addition, the algorithm that generates Q_{mf} has only one free parameter ρ , and in the $\rho=1$ case Q_{mf} becomes the square lattice.

We observe that percolation in a multifractal presents different features from percolation in a regular lattice. There are two reasons for that: the heterogeneous distribution of weight (area) among the blocks and the variation of the coordination number of the topological structure. The weight of each block in a multifractal counts differently in the mass of

the infinite percolating cluster. The difference in weight of the blocks changes the dispersion of the histogram of percolating lattices. The phenomenon of two peaks appearing in the histogram is also connected with the weight difference. We model the distance between the peaks using bimodal statistics. In the limit of $n \rightarrow \infty$ all the histograms of multifractals seem to collapse onto a single curve.

For all cases in which $\rho \neq 1$ the multifractal Q_{mf} shows a coordination number (number of neighbors of each block) that changes along the object. The average coordination number of Q_{mf} is around 5.436. In contrast, the situation $(s,r)=(1,1)$ (the particular case of the square lattice) has a coordination number constant and equal to 4. This suggests that the case $\rho \neq 1$ represents a break in the symmetry of the system. In this sense the coordination number (topology) is much more complex for Q_{mf} than for a regular lattice. De-

spite these differences, we have done numerical estimations of the fractal dimension of the percolating cluster in the multifractal, obtaining values that are around 1.89, the same dimension found for the incipient percolation cluster in a two-dimensional regular lattice. The numerical simulation of the β critical exponent also shows the same value as in the two-dimensional regular case and points to the same conclusion that we have regular percolation.

ACKNOWLEDGMENTS

The authors gratefully acknowledge the financial support of Conselho Nacional de Desenvolvimento Científico e Tecnológico (CNPq) Brazil, FINEP, and CTPETRO. We also thank D. M. Tavares for helpful comments.

-
- [1] *Fractals and Disordered Systems*, edited by A. Bunde and H. Havlin (Springer, Berlin, 1991).
 - [2] D. Stauffer and A. Aharony, *Introduction to Percolation Theory* (Taylor & Francis, London, 1994).
 - [3] H. E. Stanley *et al.*, *Physica A* **266**, 1 (1999).
 - [4] M. Sahimi, *Applications of Percolation Theory* (Taylor & Francis, Bristol, 1994).
 - [5] L. S. Lucena, J. M. Araujo, D. M. Tavares, L. R. da Silva, and C. Tsallis, *Phys. Rev. Lett.* **72**, 230 (1994).
 - [6] L. S. Lucena, L. R. da Silva, and S. Roux, *Physica A* **266**, 86 (1999).
 - [7] L. S. Lucena, L. R. da Silva, and S. Roux, *Fractals* **11**, 29 (2003).
 - [8] D. Stauffer and N. Jan, *Physica A* **277**, 215 (2000).
 - [9] M. J. Powell, *Phys. Rev. B* **21**, 3725 (1980).
 - [10] E. T. Gawlinski and H. E. Stanley, *J. Phys. A* **14**, L291 (1981).
 - [11] M. Sahimi and S. Mukhopadhyay, *Phys. Rev. E* **54**, 3870 (1996).
 - [12] M. A. Knackstedt, M. Sahimi, and A. P. Sheppard, *Phys. Rev. E* **61**, 4920 (2000).
 - [13] J. Muller, *Ann. Geophys.* **11**, 525 (1993).
 - [14] P. N. Khue, O. Fluseby, A. Saucier, and J. Muller, *J. Phys.: Condens. Matter* **14**, 2347 (2002).
 - [15] R. H. Riedi (unpublished).
 - [16] P. Hubert, *Hydrol. Sci. J.* **46**, 897 (2001).
 - [17] S. Sachs, S. Lovejoy, and D. Schertzer, *Fractals* **10**, 253 (2002).
 - [18] F. Herrmann, Ph.D. thesis, Delft University of Technology, 1997.
 - [19] S. Mukhopadhyay and M. Sahimi, *Chem. Eng. Sci.* **55**, 4495 (2000).
 - [20] J. E. de Freitas, L. S. Lucena, and S. Roux, *Physica A* **266**, 81 (1999).
 - [21] M. E. J. Newman and R. M. Ziff, *Phys. Rev. Lett.* **85**, 4104 (2000).
 - [22] J. E. de Freitas and L. S. Lucena, *IJMPC* **11**, 1581 (2000).
 - [23] J. E. de Freitas, L. S. Lucena, and S. Roux, *Phys. Rev. E* **64**, 051405 (2001).
 - [24] M. Barnsley, *Fractals Everywhere* (Academic, Boston, 1988).